Microporous and Mesoporous Materials 314 (2021) 110829

Contents lists available at ScienceDirect

Microporous and Mesoporous Materials

journal homepage: http://www.elsevier.com/locate/micromeso

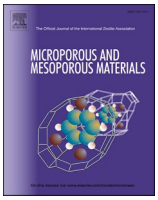

Effect of microwave assisted solvothermal process parameters on carbon dioxide adsorption properties of microporous carbon materials

P. Staciwa [a], D. Sibera [a,e], I. Pełech [a], U. Narkiewicz [a,*], W. Łojkowski [b], S. Dąbrowska [c], R. Cormia [d]

[a] Department of Chemical and Environment Engineering, Faculty of Chemical Technology and Engineering, West Pomeranian University of Technology in Szczecin, Pulaskiego 10, 70-322, Szczecin, Poland
[b] Institute of High Pressure Physics, Polish Academy of Science, Sokolowska 29/37, 01-142, Warsaw, Poland
[c] Faculty of Materials Science and Engineering, Warsaw University of Technology, Woloska 141, 02-507, Warsaw, Poland
[d] Chemistry Faculty, Chemistry Department, Foothill College, 12345 El Monte Road, Los Altos Hills, CA, 94022, USA
[e] Faculty of Civil and Environmental Engineering, West Pomeranian University of Technology in Szczecin, al. Piastów 50a, 70-311 Szczecin, Poland

ARTICLE INFO

Keywords:
Microporous carbon spheres
Solvothermal process parameters
Carbon dioxide adsorption

ABSTRACT

In this work, production and characterization of carbon spheres from resorcinol and formaldehyde, using a microwave assisted solvothermal reactor, is presented. The influence of different experimental conditions, e.g., reaction time, pressure, and power, on the structure of the obtained materials, and carbon dioxide adsorption properties, was studied.

Using the method described in this work, it is possible to significantly reduce the reaction time, to as low as 10 min, compared with widely described processes carried out in autoclaves, requiring several hours. Simultaneously, it was discovered that the application of higher reactor pressures, over 3 MPa, resulted in the destruction of spherical shape and the formation of graphitic layers.

The importance of micropores below 0.4 nm, for adsorption of carbon dioxide, was also shown in this work. Microporous carbon spheres with efficient CO_2 adsorption properties (nearly 7 mmol/g at 1 bar and 0 °C) were synthesized using this process.

1. Introduction

Combustion of fossil fuels results in emission of carbon dioxide, the major anthropogenic factor related to climate change, affecting the healthy functioning of the biosphere [1,2]. The consequences of an increase in the Earth's global temperature are, for example, species extinction, changes in the Earth's hydrologic cycle, and climate anomalies. Among the scientific community, there is significant interest in solid adsorbents that capture carbon dioxide, a promising means to address this problem.

In recent years, a number of materials have been investigated as solid state adsorbents for CO_2 and can be divided into non-carbonaceous: zeolites [3–6], silica [7–9], metal-organic frameworks and porous polymers [10,11], alkali metal [12–14], metal oxide carbonates [15,16] and carbonaceous materials: activated carbons [17,18], ordered porous carbons [19–21], activated carbon fibers [22,23], and graphene [24–26].

Carbon spheres (CSs) have attracted significant attention due to their unique chemical and physical properties: a high specific surface area, large porous volume, well defined pore size distribution, chemical stability, low cost, possibility for modification with heteroatoms, and high affinity for carbon dioxide [27–30].

Carbon spheres are also effective in removing organic pollutants [31,32], heavy metal ions, phenol, dyes [33] and nanoparticles [34]. Their potential application in energy storage [35], biomedical application, catalysis, lithium batteries [36,37], catalyst support [38,39], and drug delivery [40] has been studied as well.

There are two general approaches to the synthesis of carbon spheres. The first is based on the high-temperature decomposition of chemical substances containing carbon, including arc-discharge [41,42], laser ablation [43,44], and chemical vapor deposition methods. Synthesis of carbon spheres from a wide range of hydrocarbons, using CVD routes, both by catalytic [45] and non-catalytic [46] means, has been reported in the literature. Methane [47], and acetylene [48] have a major role as

* Corresponding author.
E-mail address: urszula.narkiewicz@zut.edu.pl (U. Narkiewicz).

https://doi.org/10.1016/j.micromeso.2020.110829
Received 2 August 2020; Received in revised form 23 November 2020; Accepted 11 December 2020
Available online 23 December 2020
1387-1811/

carbon precursors in synthesizing carbon materials.

The second approach consists of two steps. First, decomposition of organic compounds by heat treatment of solutions of materials with high carbon content, e.g. polymers, often in an autoclave, and second, pyrolysis of these materials at elevated temperatures. In this approach reactants are placed in various types of steel, Teflon lined autoclaves and usually heated to low temperatures. Compared to the methods mentioned above, hydrothermal or solvothermal treatment in an autoclave requires much less energy. A variety of carbon sources can be processed using this method, e.g., sugars [49–53], polymers [54], wastes [55], etc. Very high adsorptive properties are observed for carbon spheres obtained from resorcinol – formaldehyde resin. As reported by Liu and coworkers, carbon spheres can also be derived from RF resin using the Stöber method [56], originally developed for producing silica spheres [57]. This method requires solvents, namely water, alcohol and a base catalyst. By controlling the reactant concentrations, the diameter of the spheres can be precisely tuned. After polycondensation of the resorcinol - formaldehyde resin is initialized, the mixture is stirred for 24 h prior to hydrothermal treatment in the autoclave, where cross-linking occurs.

Despite the fact that hydrothermal treatment is the most common way to produce carbon spheres, this method has several disadvantages. First, this method takes considerable time (several hours), and second, a heat gradient in the reaction volume is an unavoidable problem that hinders production of a uniform product.

Recently, microwave irradiation has attracted more attention as a new efficient heating method [58]. This method is widely used for many applications, such as organic synthesis [59,60] or synthesis of magnetic nanoparticles [61]. This method is based on microwave irradiation affecting the particles. Compared to conventional heating in an autoclave, microwave irradiation has numerous advantages. The working principle of microwave heating is based on dielectric heating. For effective microwave heating, the presence of ions and dipoles in solution is necessary. Dipoles in solution align under the induced magnetic field. The frequency range of the microwave field (0.3–30 GHz) is appropriate to excite the polar particles in solution [62]. Oscillations of the magnetic field cause rotations of the dipoles; simultaneously, ions oscillate back and forth under magnetic field, hence collisions are induced. These rotations and collisions are responsible for heat generation in the whole volume of the reactor. As a result, the microwave reactor can perform solvothermal synthesis with a low thermal gradient.

In our previous paper [63], we reported a significant shortening of reaction time by the application of a microwave assisted reactor, compared to a conventional reaction in an autoclave. In that work, the influence of chemical activator (potassium oxalate) concentration, modification with ethylenediamine and carbonization temperature on the adsorption properties of carbon spheres was investigated. It was proved, that the optimal weight ratio of potassium to carbon is 7:1. Modification of carbon spheres with potassium oxalate and ethylenediamine simultaneously significantly enhanced carbon dioxide adsorptive properties (from 3.25 mmol/g for the unmodified sample to 5.89 mmol/g for modified). It was also shown that the highest CO_2 adsorption efficiency for those materials occurred for samples carbonized at 700 °C.

In this paper we investigated further the effect of varying reaction conditions in the production of carbon spheres from resorcinol - formaldehyde resins using a microwave assisted solvothermal reactor. The goal was also to investigate how far the pressure and power of the solvothermal reactor could be increased without destroying the structure of the carbon spheres. Three key parameters were selected to establish the optimal conditions of the method: reaction pressure, reactor power set, and time (duration) of reaction. The influence of varied experimental conditions on the structure, surface area, and porosity of the carbon spheres, and the associated carbon dioxide adsorption properties of the produced materials, was studied.

2. Materials preparation

Sample preparation was performed as follows: First, 0.6 g of resorcinol was dissolved in an aqueous alcohol solution composed of 60 ml distilled water and 24 ml of ethanol. Next, to adjust pH, 0.3 ml of ammonium hydroxide (25 wt%) was added into the solution. After that, 4.95 g of potassium oxalate was added and the mixture was stirred until the potassium oxalate was completely dissolved. The weight ratio of potassium: carbon was 7:1. Finally, 0.9 ml of formaldehyde (37 wt %) was added to the solution, and mixed using a magnetic stirrer at ambient conditions to facilitate the polycondensation reaction. After 24 h, the mixture was transferred into a microwave assisted solvothermal reactor MSS2, designed and manufactured by the Institute of High Pressure Physics of Polish Academy of Science in cooperation with Łukasiewicz Research Network - The Institute for Sustainable Technologies [64,65]. The processes were conducted under different experimental conditions, e.g. reaction time (5, 10, 15 min), pressure (1; 1,5 2; 3; 4 MPa) and generated power (1000, 1500, 2000 W). In this paper the materials obtained were denoted as RF, for example RF_1/1000/5, where the first number means the value of pressure (1 MPa), second - reactor power set (1000 W) and third - the reaction time (5 min). After treatment in the reactor, the product obtained was dried for 48 h at 80 °C and next carbonized in a high-temperature furnace (HST 12/400 Carbolite) under argon atmosphere at the temperature rising from 20 °C to 350 °C with a heating rate of 1 °C/min and holding time 2 h and from 350 °C to 700 °C with a heating rate of 1 °C/min. When a temperature of 700 °C was reached, the carbonization continued for an additional 2 h. The carbonization temperature (700 °C) was chosen based on our previous research [28,63,66]. Afterwards, the sample was cooled to room temperature under argon atmosphere. The final product was washed two times with 200 ml of distilled water and dried for 48 h at 80 °C under atmosphere.

3. Materials characterization

In experiments described in our previous papers, an Ertec Magnum II Microwave reactor was used [28,63,66,67]. However, the maximum microwave power reached in that reactor was 600 W, and we were curious about the effect of increasing power on the structure of the carbon spheres. The experiments described in the present paper were carried out in another reactor, enabling better control of the reaction parameters – a microwave solvothermal reactor MSS2 developed at the Institute of High Pressure Physics, shown in Fig. 1 [64,65]. This reactor has several advantages [65]. The MSS2 reactor also permits a rapid, uniform heating and makes a synthesis under high purity in close vessel (batch) and stop-flow mode with precise control of the reaction time and pressure. The accuracy of the reaction time is 1 s and the pressure obtained inside the vessel can reach 10 MPa. Specifically, performing the thermal treatment in the MSS2 reactor allowed for higher microwave power to be applied, from 1000 to 3000 W. The higher power resulted in reaching the set pressure faster, resulting in a shortening of the reaction time. Furthermore, the larger volume reaction vessel (270 ml of the precursor) also increases the efficiency of the entire reaction process. The reliability of this reactor type was proven in many papers, for example for the synthesis of hydroxyapatite [68] or ZnO nanoparticle [69,70]. The MSS2 reactor can work in two different synthesis modes, in stop-flow and batch mode. In this paper, results of synthesis in the batch mode are presented.

The structure of the samples was determined using a ZEISS Scanning Electron Microscope (SEM) and FEI Tecnai F20 High-Resolution Transmission Electron Microscope (HRTEM). The phase composition was investigated using X-Ray Diffraction (XRD) using Cu Kα radiation (λCu Kα = 0.1540 nm) on an Empyrean, Panalytical. Phase identification was performed using HighScore+ and the ICDD PDF-4+ 2015 database. The Raman spectra were recorded using the Renishaw InVia Raman Microscope spectrometer with excitation laser lines of 785 nm (1.58 eV).

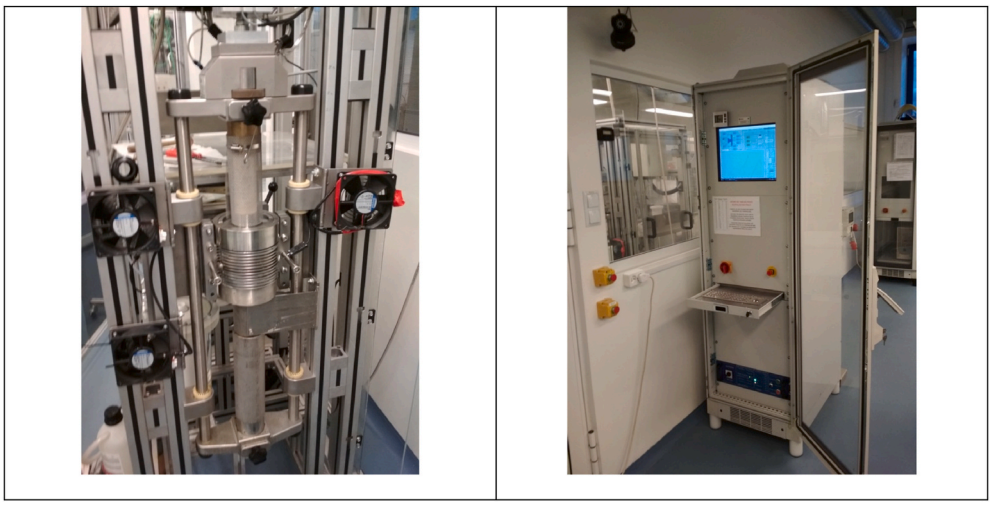

Fig. 1. Presentation of the MSS2 reactor working in the batch mode.

Thermal stability of the materials was investigated with Thermal Gravimetric Analysis (TGA), using a STA 449C thermobalance (Netzsch Company, Germany). Approximately 10 mg of the sample was heated at 10 °C/min to 950 °C under air atmosphere.

Characterization of porosity of the materials was performed using the N_2 adsorption/desorption Quadrasorb™ automatic system (Quantachrome Instruments) at −196 °C. The Brunauer–Emmett–Teller (BET) equation was used to determine surface areas (S_{BET}) in the relative pressure range of 0.05–0.2. The total pore volume, V_p, was calculated from the volume of nitrogen held at the highest relative pressure (p/p0 = 0.99). The volume of micropore, V_{mic}, was estimated using the density functional theory (DFT) and the pore-size distribution (calculated from the adsorption branch of the isotherms) using the Barrett–Joyner–Halenda (BJH) method.

Before each adsorption experiment, samples were outgassed at 250 °C under a vacuum of 1×10^{-5} mbar for 12 h to remove adsorbed species that could intervene in the adsorption processes, using a MasterPrep multi-zone flow/vacuum degasser from Quantachrome Instruments.

Carbon dioxide sorption isotherms at 0 °C and 25 °C were determined using the same Quadrasorb™ automatic system (Quantachrome Instruments) with a relative pressure range between 0 and 0.98. Pore Size Distribution (PSD) of the samples was calculated from CO_2 sorption isotherms at 0 °C using NLDFT model. The density of the materials was investigated using a Micro-Ultrapyc 1200e helium pycnometer.

4. Results and discussions

Carbon spheres were prepared using a microwave assisted solvothermal reactor and the influence of varied experimental conditions: reaction time (5, 10 and 15 min), obtained pressure (1; 1.5; 2; 3 and 4 MPa) and generated power (1000, 1500 and 2000 W) on the physical and gas adsorption properties of the materials was investigated.

The phase composition of the samples was examined using XRD. Selected diffraction patterns are presented in Fig. 2. It was observed that synthesis conditions had no significant effect on the phase composition of the obtained materials. XRD patterns exhibited the presence of two peaks: the first at 25° and second at 43°, which can be assigned to the stacking carbon layer structure (002) and ordered graphitic carbon structure (100) [71]. Broadening of the two peaks suggests a low degree of graphitization, and the possible presence of amorphous carbon [72].

Comparing XRD patterns of the samples obtained in the microwave reactor at a power set of 1000 W (Fig. 2a), a strong decrease of 002 peak intensity and increase of 100 peak intensity was observed, at a reaction pressure of 4 MPa. Additionally, a sharper 100 peak with greater intensity was detected for the sample RF_4/1000/15, which suggest the higher graphitization of carbon material. With the increase of the reaction pressure from 1 MPa to 2 MPa, the intensity of 002 peak slightly decreased.

A similar effect was observed for samples obtained with a reactor power of 2000 W (Fig. 2b). There were no noticeable differences between XRD patterns observed for the RF_1/2000/15 and RF_1.5/2000/15 materials, whereas for samples RF_2/2000/15 and RF_3/2000/15, a

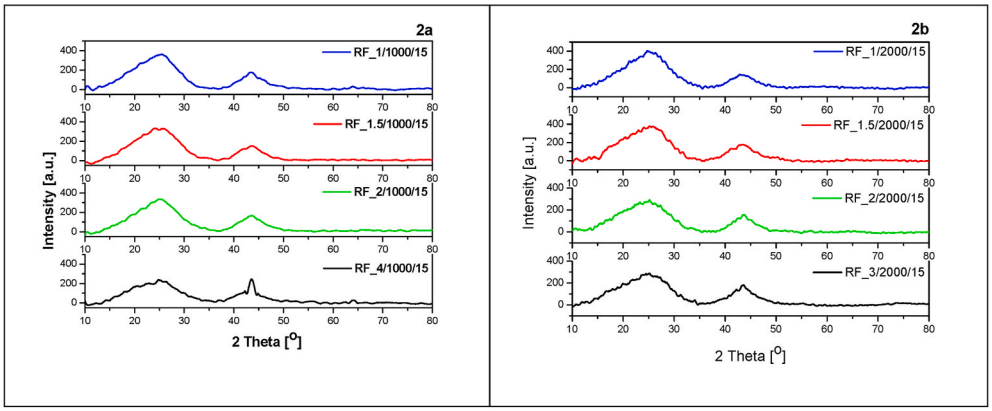

Fig. 2. Diffraction patterns of carbon materials obtained under different pressure and reactor power set 1000 W (Figs. 2a) and 2000 W (Fig. 2b).

decrease in intensity of 002 peaks was observed, which suggests a reduction of amorphous carbon and, simultaneously, an increase in degree of graphitization. It is worth noting that for material prepared under a pressure 3 MPa, the sharper peak with greater intensity was not detected. The sharpness of these peaks suggests the presence of a crystalline carbon phase within the carbon spheres [73].

Structure of the samples was investigated using Field Emission Scanning Electron Microscopy (FE-SEM), with representative SEM images presented in Fig. 3. Illustrated in Fig. 3a, 3b and 3c, are carbon materials obtained under pressures of 1 MPa, 1.5 MPa or 2 MPa and denoted as RF_1/1000/15, RF_1.5/1500/15, RF_2/2000/10, respectively, clearly showing the non-uniform size of spherical particles. Carbon spheres with diameters in the range of 1200–1500 nm and smaller – with diameters of about 200 nm were observed. Jaroniec et al. claim that the presence of smaller particles can be explained by the formation of smaller emulsion droplets containing larger amounts of ethylenediamine as a source of nitrogen [74] or in the presence of cysteine as a particle stabilizer and a source of heteroatoms (nitrogen and sulphur [75]). These emulsion droplets are converted into spheres through polymerization of resorcinol and formaldehyde and the presence of e.g. cysteine can slow down the reaction rate between resorcinol and formaldehyde, resulting in reducing the size of the emulsion droplets and in the consequence reducing other size of carbon spheres [77]. It is worth to note that the same authors did not observe similar behaviour when carbon spheres were prepared only with the addition of potassium oxalate as activating agent [76]. Scherdel et al. [77] found that small particles appeared near the gelation limit for relatively high sodium carbonate concentration, added as the catalyst, and tend to agglomerate

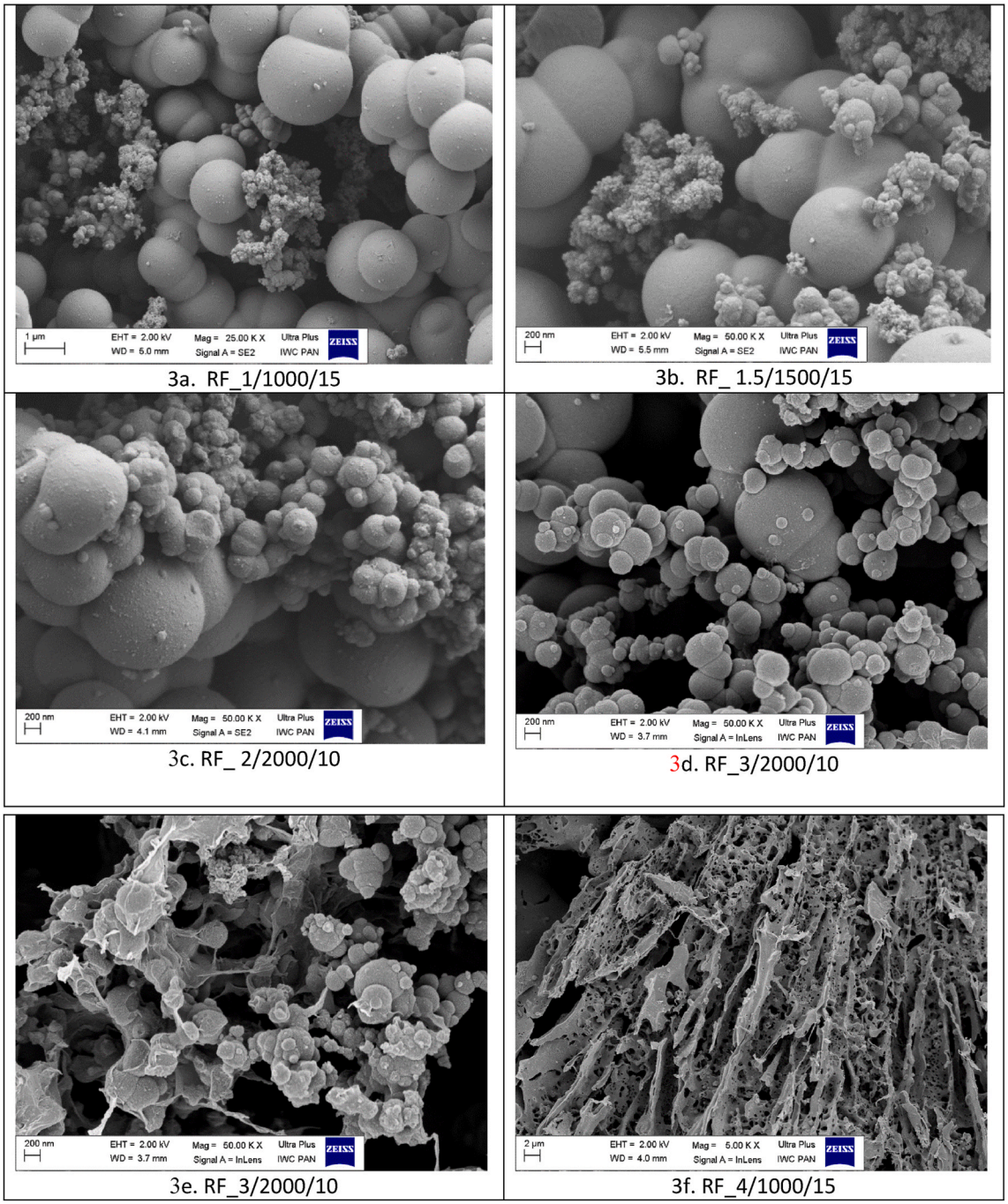

Fig. 3. SEM images of the materials obtained under different experimental conditions.

with each other.

So, we can speculate, that the reason for the appearance of carbon spheres with reduced diameter is the presence of potassium oxalate or e. g. insufficient mixing of resorcinol-formaldehyde mixture. Further research in this direction will be conducted.

Furthermore, the merging of carbon spheres was noticed. According to Ret-Raap et al. [78] the contact of the organic spheres (which have oxygenated groups on the surface) with CO_2 at high temperatures can give rise to the merging effect.

Together with the increase of reactor pressure up to 3 MPa, the spherical shape of the particles was preserved, and the structure of the carbon spheres did not change significantly (Fig. 3d), but probably some graphitic layers appeared, as shown in Fig. 3e. A higher pressure of 4 MPa resulted in collapse of the spheres, with graphitic layers clearly observed (Fig. 3f).

Structure of the samples was further investigated using High Resolution Transmission Electron Microscopy (HRTEM). HRTEM images presented in Fig. 4 confirm results obtained using Scanning Electron Microscopy (SEM). Under the pressure of 1 MPa and 2 MPa, spherical shapes with a smooth surface were observed, with diameters ranging from 1200 to 1500 nm (Fig. 4a). Under the same pressure, as reactor power increased, the surface texture becomes coarser, and flaws on the rough surface were observed (Fig. 4b). Similarly, as shown in the SEM images, for samples prepared under 4 MPa (Fig. 4c), instead of a purely spherical shape, graphitic layers are visible, indicating the process conducted at higher pressure resulted in collapse of spherical structure. As a consequence, a highly porous sponge-like carbon material with highly developed surface area was observed.

Summarizing, the microscopic studies indicated that reaction time did not play an essential role in the structure of the carbon spheres. However, increase in reactor power caused the visible changes on surface of the carbon spheres. Differences were clearly evident for samples obtained at higher pressure, and correlate well with results obtained using X-ray diffraction.

The samples were also characterized using Raman spectroscopy. The Raman spectra of the samples obtained in the microwave reactor at a power set of 1000 W for 15 min and under 10 or 40 MPa are presented in Fig. 5. The following bands were identified: G and D at ~1580 cm^{-1} and ~1310 cm^{-1}, respectively. The first peak is related to the vibration of the sp^2-hybridized carbon atoms in the graphite layer, the second - is usually attributed to the presence of amorphous carbon or associated with the vibration of carbon atoms with dangling bonds in the plane with termination by disordered graphite. It is also known that the intensity ratio between the D and G peaks (I_D/I_G) gives useful information

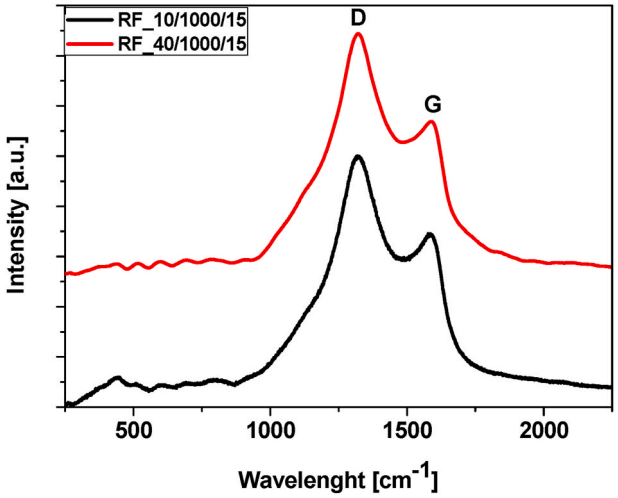

Fig. 5. Raman spectra of the samples prepared at lower (1 MPa) and higher (4 MPa) reaction pressure.

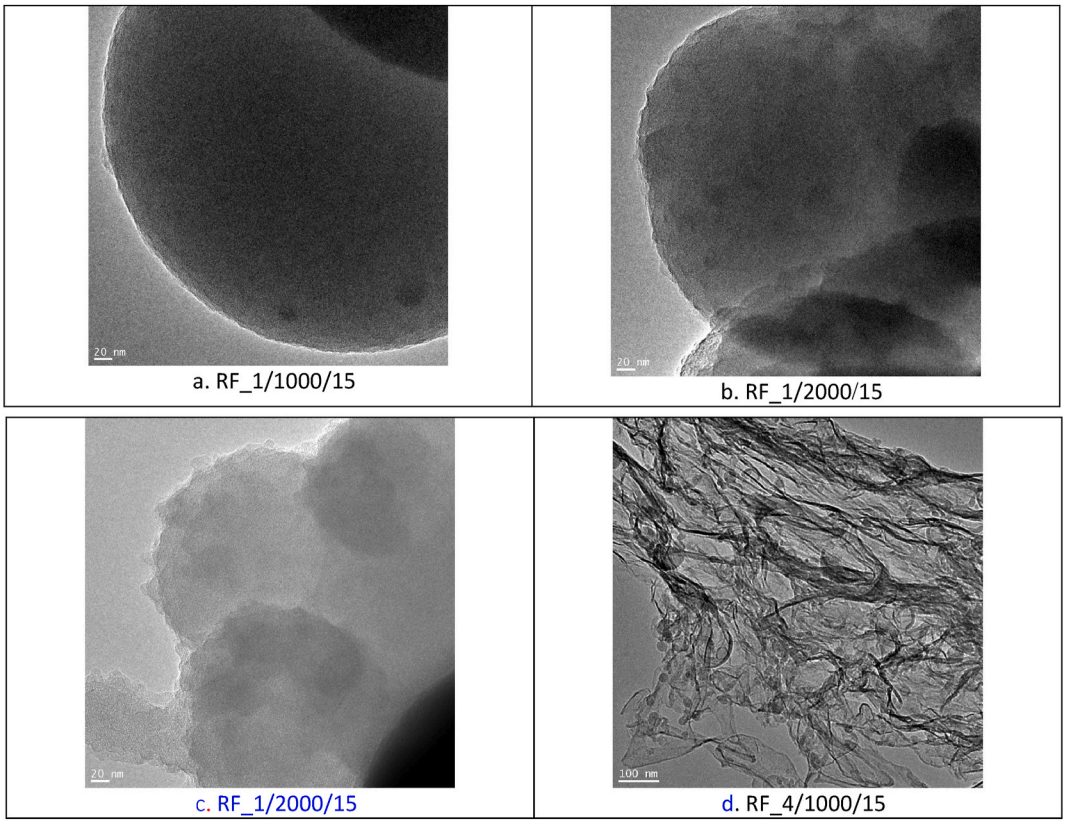

Fig. 4. High-resolution transmission electron microscopy (HRTEM) images of the samples prepared at lower (1 MPa) and higher (4 MPa) reaction pressure.

on the graphitization degree or the lattice distortion of carbon based materials. The intensity ratios of I_D/I_G for RF 10/1000/15 and RF 40/1000/15 samples were calculated to be 1.35 and 1.26, respectively. The decrease of I_D/I_G together with the increase of the reaction pressure can indicate that the graphitization of the sample increased, implying the formation of more ordered structure. It is in accordance with the results obtained using X-ray diffraction method and transmission electron microscopy presented above.

Thermal stability of the samples was studied using thermogravimetric analysis (TGA). The thermogravimetric curves are presented in Fig. 6 and confirm that the materials produced in this study are composed of multiple forms of carbon that undergo combustion at different temperatures. The first weight loss at a temperature of approximately 100 °C was associated with evaporation of water. The second step taking place between 100 °C and 350 °C can be assigned to the removal of functional groups. The last step occurs between 350 °C and 550 °C and is ascribed to oxidation of the carbon skeleton with a low degree of graphitization [79]. Due to numerous active centers, amorphous carbon is already oxidized at temperatures in the range of 400–500 °C [80,81]. The oxidation of these samples had already started at 350 °C, which may indicate the significant amount of amorphous carbon in the samples.

In the case of the samples obtained where reactor power set was 1000 W, the effect of reaction pressure on the thermal stability of materials was negligible, while for processes with the reactor power of 1500 W or 2000 W, together with the increase of the reaction pressure, a slight improvement in the thermal stability of the materials was observed. This is likely associated with a higher graphitic content in those samples, as suggested by both X-Ray Diffraction (XRD) and Scanning Electron Microscopy (SEM), as described above. Interestingly, an increase of microwave power from 1000 to 2000 W at constant pressure resulted in a decrease of the material's thermal stability.

As was stated above in case of HRTEM studies, for the samples obtained at higher reactor power the rough surface was observed. So we can deduce that the amount of non-graphitic carbon increased and simultaneously the decrease of thermal stability of the sample could be noticed.

The specific surface area of the composites was measured by physical adsorption of N_2 at −196 °C using a Quadrasorb™ apparatus. Before each measurement, all samples were degassed under vacuum at 250 °C for 12 h. The specific surface area was determined by the adsorption isotherm over a relative pressure (P/P_0) in the range of 0.05–0.20. The total pore volume, V_p, including both micropores and mesopores, was estimated by converting the amount of N_2 gas adsorbed at a relative pressure of 0.99 to liquid volume of the adsorbate (N_2). The results are shown in Table 1.

Fig. 7 shows typical nitrogen adsorption isotherms of three typical samples. For the materials produced under different conditions, similar nitrogen isotherms were observed. A visible increase of the adsorption rate at the end of the isotherms can suggest that the macropores are present in materials, hence the adsorption isotherms are type II characteristic for the macroporous materials [82]. Compared to results from

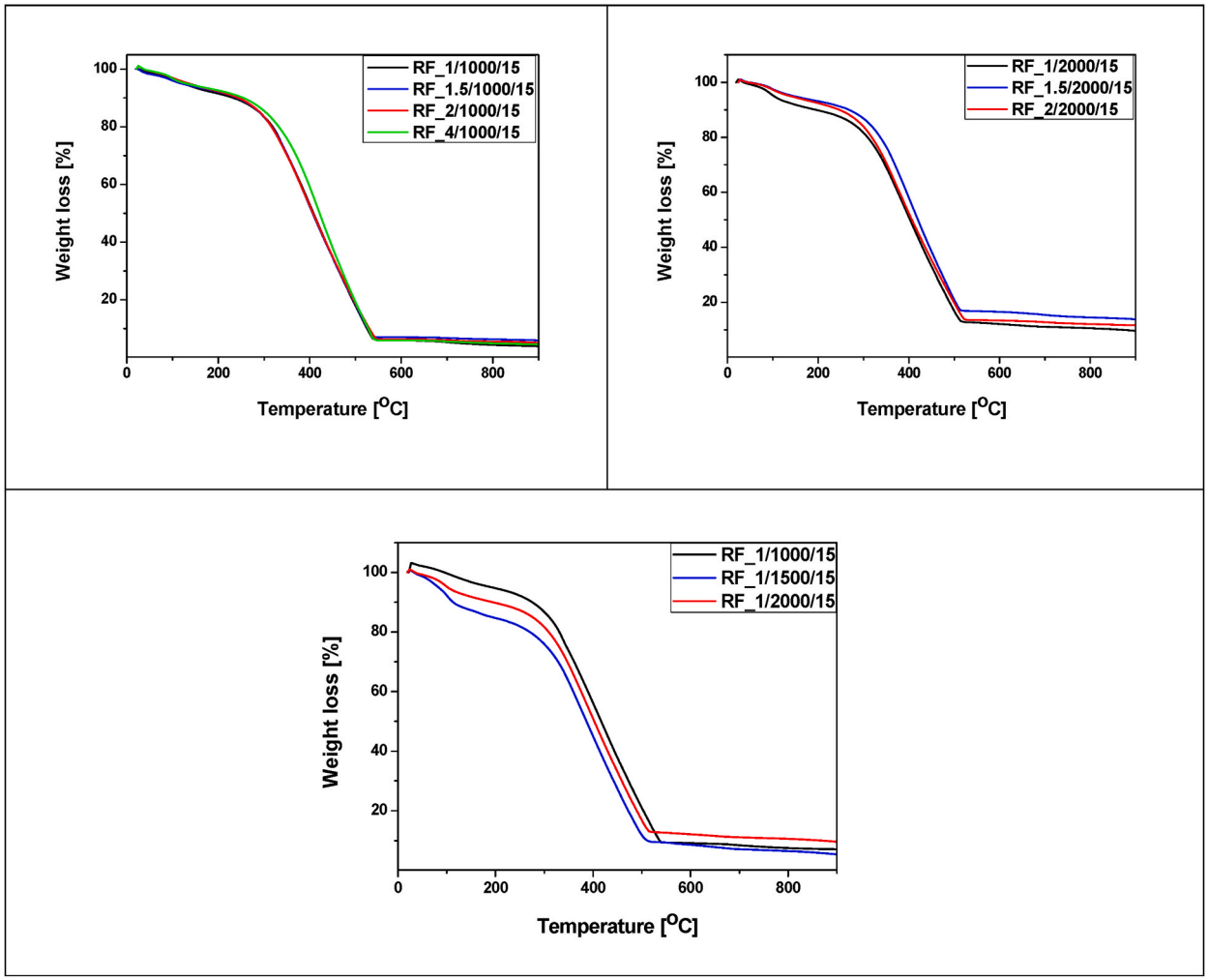

Fig. 6. Thermal stability of the tested samples.

Table 1
Physicochemical properties of the tested samples.

Sample	Density	S_{BET}	TPV	V_m	V_u	V_s	CO_2 adsorption at 0 °C	CO_2 adsorption at 25 °C
	(g/cm^3)	(m^2/g)	(cm^3/g)	(cm^3/g)	(cm^3/g)	(cm^3/g)	(mmol/g)	(mmol/g)
RF_1/1000/15	1.80	1244	0.58	0.483	0.188	0.295	6.45	3.52
RF_1/1500/15	1.79	1096	0.48	0.444	0.150	0.294	6.47	3.32
RF_1/2000/15	1.80	1172	0.51	0.462	0.155	0.307	6.72	3.65
RF_1.5/1000/15	1.76	1188	0.50	0.466	0.202	0.264	5.57	3.65
RF_1.5/1500/15	1.73	1167	0.50	0.458	0.181	0.277	6.14	4.06
RF_1.5/2000/15	1.77	1207	0.56	0.468	0.161	0.307	6.61	3.85
RF_2/1000/15	1.84	1177	0.54	0.469	0.193	0.276	5.53	3.93
RF_2/1500/15	1.78	1164	0.53	0.460	0.154	0.306	6.65	4.18
RF_2/2000/15	1.75	1148	0.50	0.452	0.162	0.290	6.30	4.07
RF_3/2000/15	1.81	1216	0.51	0.476	0.174	0.302	6.51	3.94
RF_4/1000/15	1.69	1376	0.58	0.522	0.250	0.272	5.65	4.33
RF_1/2000/5	1.79	1124	0.50	0.461	0.177	0.284	6.26	4.13
RF_1/2000/10	1.77	1151	0.48	0.455	0.144	0.311	6.81	4.27
RF_1.5/2000/5	1.76	1234	0.47	0.452	0.179	0.273	6.17	4.30
RF_1.5/2000/10	1.73	1232	0.50	0.467	0.161	0.306	6.66	4.28
RF_2/2000/5	1.75	1202	0.49	0.473	0.168	0.305	6.65	4.23
RF_2/2000/10	1.79	1464	0.62	0.591	0.277	0.314	6.99	4.13

TPV – total pore volume; Vm – Micropore volume; V_u – Ultramicropore volume (0.7–2 nm); V_s – Supermicropore volume (<0.7 nm).
The micropore, ultramicropore and supermicropore volume was calculated from N_2 adsorption isotherms at −196 °C and from CO_2 adsorption isotherms at 0 °C.

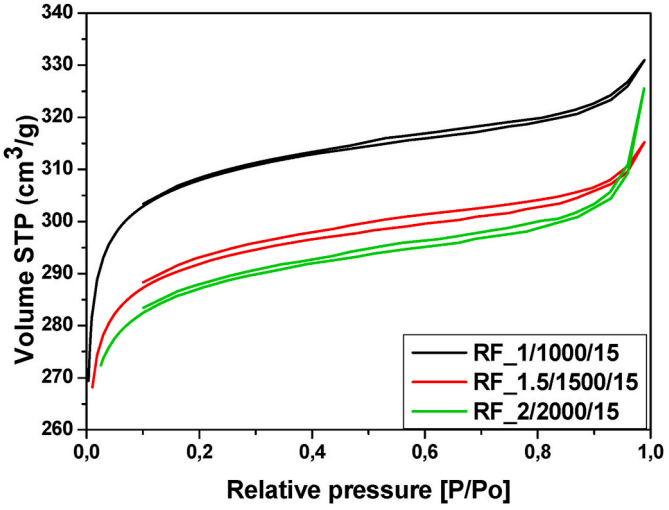

Fig. 7. Exemplary nitrogen adsorption isotherms for obtained materials.

our previous paper, where the adsorption isotherms were of the pure I type, a significant increase in macropores was noticed, and lower values of total pore volume were also observed [63]. The physicochemical properties of the samples were gathered in Table 1. For nearly all samples produced under different reaction conditions, (pressure, power, reaction time) the specific surface area and total pore volume values were similar and no correlation to reaction conditions could be observed, except the samples RF_2/2000W/10 and RF_4/1000/15. In addition, we observed that the change in structure from spherical to spongy, did not affect the magnitude of the specific surface area, or the distribution of pores in the samples. In all the samples the contribution of micropores is dominant. Moreover, the density values of the samples were scattered and no correlation was detected depending on different reaction conditions. The influence of synthesis parameters was instead observed in the CO_2 adsorption.

The sample RF_2/2000/10 showed the highest CO_2 uptake at 0 °C, what can be assigned to the highest content of supermicropores. On the other hand, the sample RF_1.5/1000/15, with the lowest content of supermicropores, adsorbed the lowest value of CO_2 molecules at 0 °C. Then, the higher content of supermicropores, the higher CO_2 adsorption at 0 °C.

In our previous work, we produced samples in the ERTEC Magnum II microwave reactor [28,63,67], and proved in that work, that using a microwave reactor can significantly reduce the reaction time compared to reactions (carbon sphere synthesis) performed in an autoclave. Furthermore, by tuning the preparation conditions, materials with higher CO_2 adsorption properties (6.21 mmol/g at 0 °C and 1 bar) could be obtained. However, the maximum microwave power that could be applied using this reactor was 600 W. In the present paper, use of the MSS2 microwave reactor enabled us to synthesise samples at different time, pressure and power conditions. Almost all samples in this work exhibited high CO_2 adsorptive properties, above 6 mmol/g and 4 mmol/g at 0 °C and 25 °C respectively.

Comparison of gas adsorption data from samples obtained at different reaction pressures, showed that with an increase of reaction pressure, the CO_2 adsorption values at 25 °C also increased (Fig. 8). For CO_2 adsorption values at 0 °C, a reverse tendency could be observed. The differences were probably due to the influence of micropores and to the increasing contribution of chemisorption in relation to physisorption. With an increase of temperature the transition from physisorption to chemisorption is observed [83]. Then, the possible explanation of the observed phenomenon can be that at 25 °C the contribution of chemisorption in relation to physisorption is higher than at 0 °C.

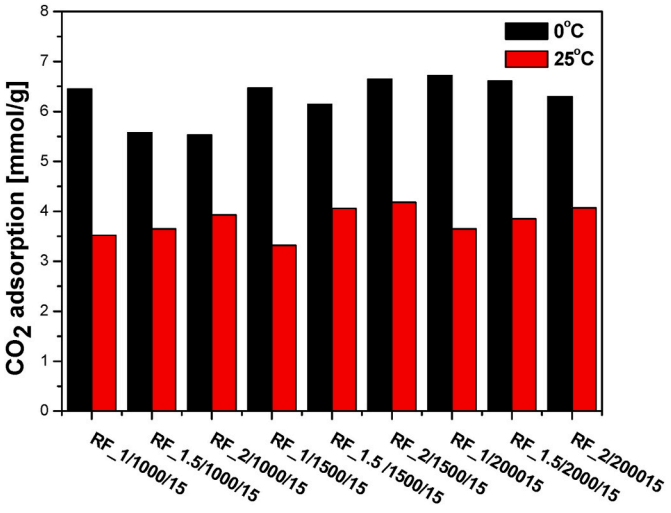

Fig. 8. Correlation between the reaction pressure and the CO_2 adsorption.

In one of our previous papers [84] we described the CO_2 adsorption studies on commercial activated carbon (pure and modified with KOH) performed using temperature-programmed desorption method (TPD-CO_2) under atmospheric pressure at three different temperatures: −30, 0 and 20 °C. At the temperature of −30 °C the adsorption energy calculated was equal to 25.8 and 26.9 kJ/mol on the unmodified and modified with KOH activated carbon, respectively, which was ascribed to physisorption. With increasing temperature, adsorption at 0 °C and 20 °C occurred with a bond strength of 46–58 and 54–75 kJ/mol, respectively. It allowed to state that at higher temperatures the adsorption of carbon dioxide on activated carbon had a mixed (physical/chemical) character and that two types of adsorption sites are present at the surface. At 20 °C the contribution of chemisorption in relation to physisorption was higher than at 0 °C.

As shown in Fig. 9, an increase in reaction power resulted in an increase in CO_2 adsorption values at 0 °C. The lowest CO_2 adsorption values at the temperature 0 °C were gathered for the materials obtained using 1000 W. For the adsorption at 25 °C the values are scattered. Increasing the reaction power, the reactor reached faster set temperature, so the material was inside reactor for the shorter period of time. This could have an influence on the textural properties of the material, i.e. porosity and maybe on the presence of the functional groups on the surface of material.

The effect of the reaction duration on gas adsorption was investigated, and as shown in Fig. 10, no obvious tendency can be noticed.

Due to diffusional problems of the adsorptive molecules inside micropores, low temperature N_2 adsorption is not a suitable method for the investigation of microporosity of carbon materials. The higher kinetic energy of CO_2 molecules at 0 °C allows the gas to penetrate the narrower pores [85]. In order to investigate the microporosity of materials, a NLDFT model based on the CO_2 adsorption isotherms data at 0 °C was used.

According to the literature, there is a strong correlation between microporosity of carbon materials and the efficiency of CO_2 adsorption [86–88]. In a paper by Sevilla and Fuertes, high CO_2 adsorption capacity of 4.8 mmol/g at 25 °C and 1 atm, was assigned to the presence of narrow micropores below 1 nm [89]. Lee and Park claimed that the efficient CO_2 adsorption was related more to the presence of micropores of 0.7 nm diameter than to the surface area or total micropore volume [90].

The importance of narrow micropores in carbon materials derived from phenolic resins in gas adsorption was also discussed by Wickramarante and coworkers who claimed the remarkable adsorption capacity of their material (8.9 mmol/g at 0 °C and 1 atm) was related to the presence of very high contribution of micropores, below 0.8 nm [91,92].

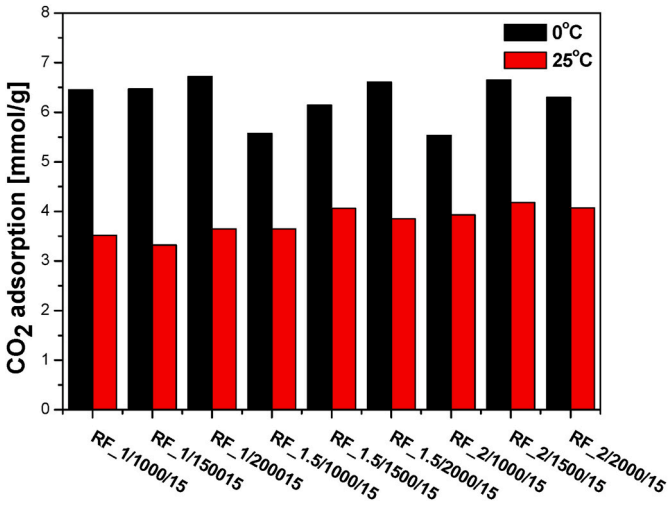

Fig. 9. Correlation between heating power and CO_2 adsorption.

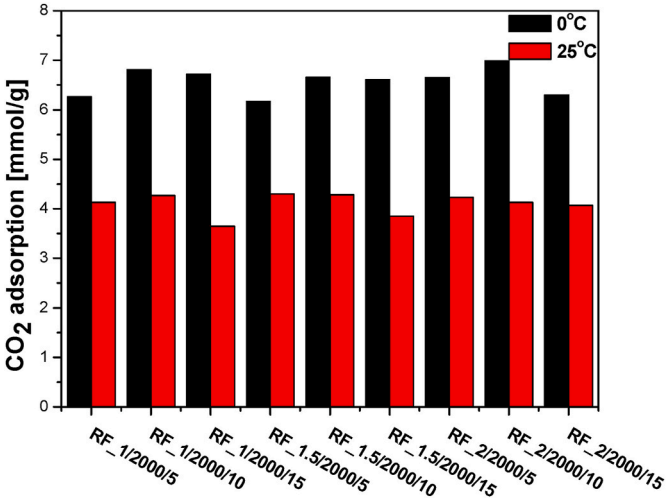

Fig. 10. Correlation between the reaction time and the CO_2 adsorption.

An interesting investigation of cooperative CO_2 adsorption was presented in the work by Chen and Watanabe [93]. A simulation showed that the highest adsorption density, at a pressure of 1 atm, was determined for slit pores in a size from 0.4 nm to 1.2 nm. The kinetic diameter of CO_2 molecule is 0.33 nm [94], thus pores below this size are not able to adsorb CO_2 molecules. The highest adsorption density was calculated for the 0.4 nm slit pores. However, at ambient conditions the most efficient CO_2 adsorption efficiency was observed in pores of size similar to the size of CO_2 molecule [95]. The presence of narrow micropores is highly desirable due to the overlapping potential fields from both sides of the pores, which results in higher CO_2 adsorption density. In our previous paper it was shown that the presence of micropores below 0.4 nm had a crucial impact on CO_2 adsorption [63]. Modification of the carbon material with potassium oxalate (to reach K:C ratio equal 7:1) resulted (in the case of the sample carbonized at 700 °C) in an increase of specific surface area of 45% and of the total porosity of 72%. Simultaneously and surprisingly, density of the material increased as well, of 10%. We explained that density increase by the content of remaining potassium, proved also by XPS measurements. What was the most important, the accompanying increase of carbon dioxide uptake reached 58% at 0 °C and 51% at 25 °C.

For materials produced in this work, almost all conditions produced three sizes of pores, and in almost all cases, a high proportion of 0.35 nm pores was observed. Given the kinetic diameter of CO_2 molecule (0.33 nm) this pore size plays a crucial role in CO_2 adsorption at ambient conditions.

All samples prepared in this study produced a high volumetric proportion of micropores below 0.7 nm, which led to high CO_2 adsorption values. Nonetheless, the effect of narrow pores below 0.4 nm on CO_2 adsorption was also considered. Sample data presented in Fig. 11a correlate with high CO_2 adsorption at 0 °C and very high content of micropores below 0.4 nm. The lowest CO_2 adsorption at 0 °C was observed for sample RF_1/2000/5, which also exhibited the lowest content of micropores below 0.4 nm. The highest values of CO_2 adsorption at 0 and 25 °C were observed for the sample prepared with a reaction time of 10 min. As shown in Fig. 11b, sample RF_1.5/1000/15, with a lack of pores below 0.4 nm, expressed much lower CO_2 adsorption at 0 °C. Also shown in Fig. 11c, there is a correlation between the presence of pores below 0.4 nm, and efficient CO_2 adsorption. Sample RF_2/1000/15 expressed a very low content of pores below 0.4 nm, and the CO_2 adsorption at 0 °C was lower - 5.53 mmol/g. Nevertheless, the adsorption at 25 °C was at an acceptable level, 3.93 mmol/g. It is worth noting that sample RF_4/1000/15 (Fig. 11d), which didn't contain pores below 0.4 nm, had the highest surface area (1376 m^2/g). Thus, the lack of micropores below 0.4 nm had an impact on the CO_2 adsorption at 0 °C

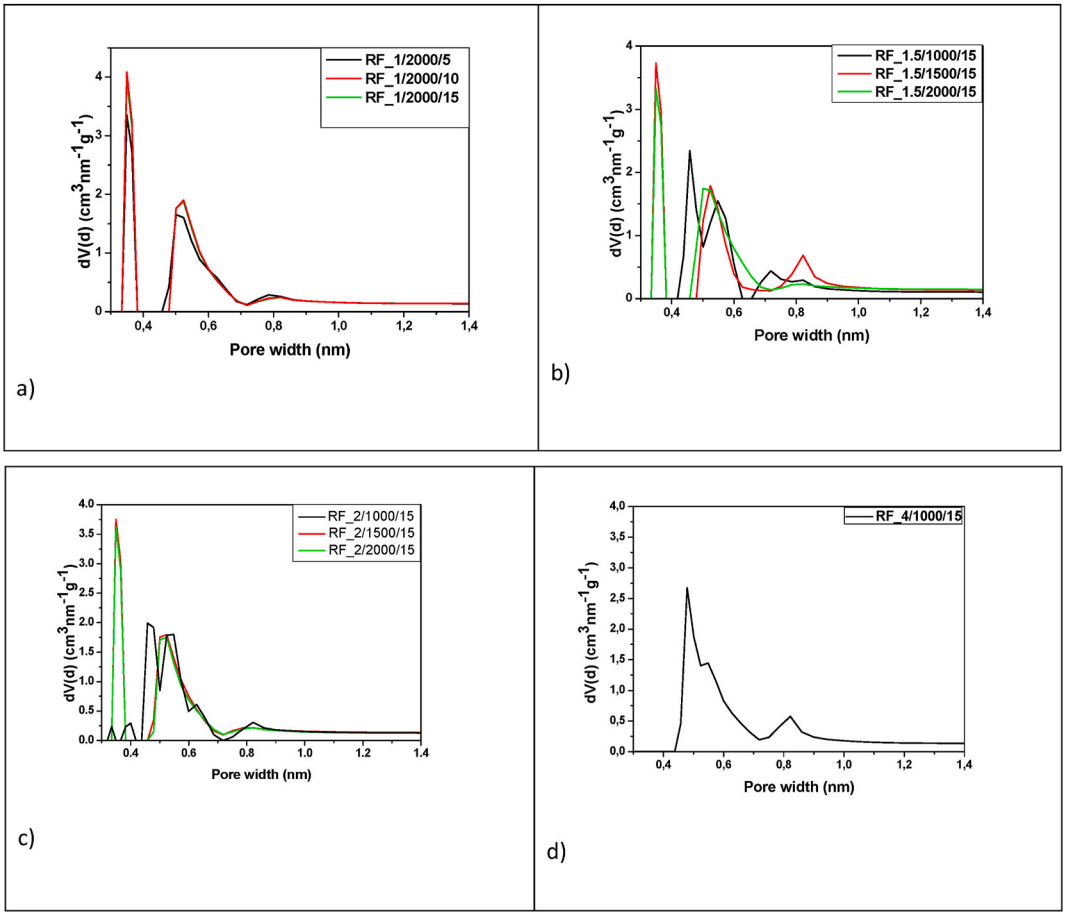

Fig. 11. PSD of the samples prepared in different conditions.

(where physisorption dominates). This sample expressed the highest content of pores in size 0.5 nm, and CO_2 adsorption at 25 °C reached 4.33 mmol/g, which was the highest value of all samples. Then, we can conclude that the presence of micropores with diameter comparable to the diameter of CO_2 molecule (0.33–0.4 nm) is favourable for physisorption (more important at 0 °C, than at 25 °C), where the presence of micropores with size above 0.5 nm is favourable for chemisorption at 25 °C.

5. Conclusions

Microporous carbon spheres with high CO_2 adsorption properties were obtained using a high pressure variable power modified Stöber method in a microwave assisted solvothermal reactor. With an increase in reaction pressure, partial transformation of spherical to polyhedral shape can be noticed, associated with a more ordered graphitic structure. No carbon spheres were produced if the reaction pressure was above 3 MPa. A significant correlation between efficient CO_2 adsorption at 0 °C and presence of pores below 0.4 nm was observed. The most efficient CO_2 carbon adsorbents were produced when the reaction time was 10 min, and reaction power was 2000 W. An increase in reaction pressure produced a higher content of graphitic structure in the material together with the collapse of the spherical shape. The accompanying changes in micropore structure were observed simultaneously for the sample prepared at 4 MPa – a disappearance of micropores below 0.4 nm, having a negative effect for carbon dioxide physisorption, but an increase in contribution of micropores of about 0.5 nm, favourable for CO_2 chemisorption occurring more intensively at 25 °C.

CRediT authorship contribution statement

P. Staciwa: sample preparation, characterization, manuscript preparation. **D. Sibera:** sample preparation, characterization, manuscript preparation. **I. Pełech:** sample preparation, characterization, manuscript preparation. **U. Narkiewicz:** manuscript preparation. **W. Łojkowski:** consultations. **S. Dąbrowska:** synthesis in microwave reactor. **R. Cormia:** consultations, manuscript preparation, proofreading.

Declaration of competing interest

The authors declare that they have no known competing financial interests or personal relationships that could have appeared to influence the work reported in this paper.

Acknowledgments

The authors acknowledge:
1) the support from the National Science Centre, Poland, with OPUS 17 grant 2019/33/B/ST8/02044.
2) Jan Mizeracki from the Institute of High Pressure Physics PAS in Warsaw for his help in gathering high quality SEM images.

References

[1] J. Lelieveld, K. Klingmüller, A. Pozzer, R.T. Burnett, A. Haines, V. Ramanathan, Effects of fossil fuel and total anthropogenic emission removal on public health and climate, Proc. Natl. Acad. Sci. 116 (2019) 7192–7197, https://doi.org/10.1073/pnas.1819989116.

[2] S. Solomon, G. Plattner, R. Knutti, P. Friedlingstein, Irreversible climate change due to carbon dioxide emissions, Proc. Natl. Acad. Sci. 106 (2009) 1704–1709, 10.1073/pnas.0812721106.

[3] W. Morris, N. He, K.G. Ray, P. Klonowski, H. Furukawa, I.N. Daniels, Y. A. Houndonougbo, M. Asta, O.M. Yaghi, B.B. Laird, A combined experimental-computational study on the effect of topology on carbon dioxide adsorption in zeolitic imidazolate frameworks,, J. Phys. Chem. C 116 (2012) 24084–24090, https://doi.org/10.1021/jp307170a.

[4] W. Cai, T. Lee, M. Lee, W. Cho, D.Y. Han, N. Choi, A.C.K. Yip, J. Choi, Thermal structural transitions and carbon dioxide adsorption properties of zeolitic imidazolate framework-7 (ZIF-7), J. Am. Chem. Soc. 136 (2014) 7961–7971, https://doi.org/10.1021/ja5016298.

[5] P. Zhao, G.I. Lampronti, G.O. Lloyd, E. Suard, S.A.T. Redfern, Direct visualisation of carbon dioxide adsorption in gate-opening zeolitic imidazolate framework ZIF-7, J. Mater. Chem. A 2 (2014) 620–623, https://doi.org/10.1039/c3ta13981f.

[6] F. Su, C. Lu, CO_2 capture from gas stream by zeolite 13X using a dual-column temperature/vacuum swing adsorption, Energy Environ. Sci. 5 (2012) 9021–9027, https://doi.org/10.1039/c2ee22647b.

[7] F.C. de Carvalho, P.F. do Nascimento, M.R.O. de Souza, A.S. Araujo, The efficiency of bimodal silica as a carbon dioxide adsorbent for natural gas treatment,, Processes 8 (2020) 289–302, 10.3390/pr8030289.

[8] Y. Zhao, Y. Shen, L. Bai, Effect of chemical modification on carbon dioxide adsorption property of mesoporous silica, J. Colloid Interface Sci. 379 (2012) 94–100, https://doi.org/10.1016/j.jcis.2012.04.064.

[9] G. Zhao, B. Aziz, N. Hedin, Carbon dioxide adsorption on mesoporous silica surfaces containing amine-like motifs, Appl. Energy 87 (2010) 2907–2913, https://doi.org/10.1016/j.apenergy.2009.06.008.

[10] W. Wang, M. Zhou, D. Yuan, Carbon dioxide capture in amorphous porous organic polymers, J. Mater. Chem. A 5 (2017) 1334–1347, https://doi.org/10.1039/c6ta09234a.

[11] L.B. Sun, Y.H. Kang, Y.Q. Shi, Y. Jiang, X.Q. Liu, Highly selective capture of the greenhouse gas CO_2 in polymers, ACS Sustain. Chem. Eng. 3 (2015) 3077–3085, https://doi.org/10.1021/acssuschemeng.5b00544.

[12] M.J. Ramírez-Moreno, I.C. Romero-Ibarra, J. Ortiz- Landeros, H. Pfeiffer, Alkaline, Alkaline-Earth Ceramic, Oxides for CO_2 capture, separation and subsequent catalytic chemical conversion, CO_2 sequestration valorization. https://doi.org/10.5772/57444, 2014.

[13] A. Salituro, A. Westwood, A. Ross, R. Brydson, Sustainable and regenerable alkali metal-containing carbons derived from seaweed for CO_2 post-combustion capture, Sus. Chem. 1 (2020) 33–48, https://doi.org/10.3390/suschem1010003.

[14] K. Upendar, A. Sri Hari Kumar, N. Lingaiah, K.S. Rama Rao, P.S. Sai Prasad, Low-temperature CO_2 adsorption on alkali metal titanate nanotubes, Int. J. Greenh. Gas Control 10 (2012) 191–198, https://doi.org/10.1016/j.ijggc.2012.06.008.

[15] S. Kumar, S.K. Saxena, A comparative study of CO_2 sorption properties for different oxides, Mater. Renew. Sustain, Energy 3 (2014) 1–15, https://doi.org/10.1007/s40243-014-0030-9.

[16] F. Karadas, C.T. Yavuz, S. Zulfiqar, S. Aparicio, G.D. Stucky, M. Atilhan, CO_2 adsorption studies on hydroxy metal carbonates $M(CO_3)x(OH)y$ (M = Zn, Zn-Mg, Mg, Mg-Cu, Cu, Ni, and Pb) at high pressures up to 175 bar, Langmuir 27 (2011) 10642–10647, https://doi.org/10.1021/la201569m.

[17] H.G. Ibrahim, M.A. Al-Meshragi, Experimental study of adsorption on activated carbon for CO_2 capture, Intech (2019) 1–20, https://doi.org/10.5772/57353.

[18] K. Tomas, F. Karel, An adsorption of carbon dioxide on activated carbon controlled by temperature swing adsorption, AIP Conf. Proc. 1889 (2017), https://doi.org/10.1063/1.5004357, 020023.

[19] G. Qin, Y. Zhang, W. Wei, Facile synthesis of a nitrogen-doped carbon membrane for CO2 capture, Mater. Lett. 209 (2017) 75–77, https://doi.org/10.1016/j.matlet.2017.07.100.

[20] N. Omidfar, A. Mohamadalizadeh, S.H. Mousavi, Carbon dioxide adsorption by modified carbon nanotubes, Technology 10 (2015) 885–892, https://doi.org/10.1002/apj.

[21] M.M. Gui, Y.X. Yap, S.P. Chai, A.R. Mohamed, Multi-walled carbon nanotubes modified with (3-aminopropyl)triethoxysilane for effective carbon dioxide adsorption, Int. J. Greenh. Gas Control 14 (2013) 65–73, https://doi.org/10.1016/j.ijggc.2013.01.004.

[22] Y. Chiang, C. Yeh, C. Weng, Carbon dioxide adsorption on porous and functionalized activated carbon fibers, Appl. Sci. 9 (2019) 1977–1992, https://doi.org/10.3390/app9101977.

[23] Y. Chiang, W. Hsu, S. Lin, R. Juang, Enhanced CO_2 adsorption on activated carbon fibers grafted with nitrogen-doped carbon nanotubes, Materials (Basel) 10 (2017) 1–12, https://doi.org/10.3390/ma10050511.

[24] F.H.B. Baldovino, N.P. Dugos, S.A. Roces, A.T. Quitain, T. Kida, Process optimization of carbon dioxide adsorption using nitrogen-functionalized graphene oxide via response surface methodology approach, ASEAN J, Chem. Eng. 17 (2017) 106–113, https://doi.org/10.22146/ajche.49559.

[25] K. Takeuchi, S. Yamamoto, Y. Hamamoto, Y. Shiozawa, K. Tashima, H. Fukidome, T. Koitaya, K. Mukai, S. Yoshimoto, M. Suemitsu, Y. Morikawa, J. Yoshinobu, I. Matsuda, Adsorption of CO2 on graphene: a combined TPD, XPS, and vdW-DF study,, J. Phys. Chem. C 121 (2017) 2807–2814, https://doi.org/10.1021/acs.jpcc.6b11373.

[26] A.A. Alghamdi, A.F. Alshahrani, N.H. Khdary, F.A. Alharthi, H.A. Alattas, S.F. Adil, Enhanced CO2 adsorption by nitrogen-doped graphene oxide sheets (N-GOs) prepared by employing polymeric precursors, Materials (Basel) 11 (2018) 578–592, https://doi.org/10.3390/ma11040578.

[27] N.K. Tripathi, Porous carbon spheres: recent developments and applications, AIMS Mater. Sci. 5 (2018) 1016–1052, https://doi.org/10.3934/MATERSCI.2018.5.1016.

[28] D. Sibera, U. Narkiewicz, J. Kapica, J. Serafin, B. Michalkiewicz, R.J. Wróbel, A. W. Morawski, Preparation and characterisation of carbon spheres for carbon dioxide capture, J. Porous Mater. (2018) 1–9, https://doi.org/10.1007/s10934-018-0601-8.

[29] J. Choma, M. Kloske, A. Dziura, K. Stachurska, M. Jaroniec, Preparation and studies of adsorption properties of microporous carbon spheres, Eng. Prot. Environ 19 (2016) 169–182, https://doi.org/10.17512/ios.2016.2.1.

[30] N.P. Wickramaratne, M. Jaroniec, Activated carbon spheres for CO2 adsorption, ACS Appl. Mater. Interfaces 5 (2013) 1849–1855, https://doi.org/10.1021/am400112m.

[31] C. Zhu, X. Chen, J. Ma, C. Gu, Q. Xian, T. Gong, C. Sun, Carbon nitride-modified defective TiO2−x@Carbon spheres for photocatalytic H2 evolution and pollutants removal: synergistic effect and mechanism insight, 20444-20458, https://doi.org/10.1021/acs.jpcc.8b06624, 2018.

[32] C. Yin, Y. Wei, F. Wang, Y. Chen, X. Bao, Magnetic hierarchical porous carbon sphere prepared for removal of organic pollutants in water, Mater. Lett. 104 (2013) 64–67, https://doi.org/10.1016/j.matlet.2013.03.143.

[33] F. Huang, C. Lee, Y. Han, W. Chao, H. Chao, Preparation of activated carbon using micro-nano carbon spheres through chemical activation, J. Taiwan Inst. Chem. Eng 45 (2014) 2805–2812, https://doi.org/10.1016/j.jtice.2014.08.004.

[34] J. Kumar, R. Mallampati, A. Adin, S. Valiyaveettil, Functionalized carbon spheres for extraction of nanoparticles and catalyst support in water, ACS Sustain. Chem. Eng. 2 (2014) 2675–2682, https://doi.org/10.1021/sc5004242.

[35] B. Zielinska, B. Michalkiewicz, X. Chen, E. Mijowska, R.J. Kaleńczuk, Pd supported ordered mesoporous hollow carbon spheres (OMHCS) for hydrogen storage, Chem. Phys. Lett. 647 (2016) 14–19, https://doi.org/10.1016/j.cplett.2016.01.036.

[36] E.S. Shin, M.S. Kim, W. Il Cho, S.H. Oh, Sulfur/graphitic hollow carbon sphere nano-composite as a cathode material for high-power lithium-sulfur battery, Nanoscale Res. Lett. 8 (2013) 1–8, https://doi.org/10.1186/1556-276X-8-343.

[37] J. Yao, T. Mei, Z. Cui, Z. Yu, K. Xu, X. Wang, Hollow carbon spheres with TiO2 encapsulated sulfur and polysulfides for long-cycle lithium-sulfur batteries, Chem. Eng. J. 330 (2017) 644–650, https://doi.org/10.1016/j.cej.2017.08.006.

[38] H. Wang, W. Wang, Y.Y. Xu, S. Dong, J. Xiao, F. Wang, H. Liu, B.Y. Xia, Hollow nitrogen-doped carbon spheres with Fe3O4 nanoparticles encapsulated as a highly active oxygen-reduction catalyst, ACS Appl. Mater. Interfaces 9 (2017) 10610–10617, https://doi.org/10.1021/acsami.6b15392.

[39] I. Nongwe, V. Ravat, R. Meijboom, N.J. Coville, Efficient and reusable Co/nitrogen doped hollow carbon sphere catalysts for the aerobic oxidation of styrene, Appl. Catal. Gen. 466 (2013) 1–8, https://doi.org/10.1016/j.apcata.2013.06.014.

[40] X. Huang, S. Wu, X. Du, Gated mesoporous carbon nanoparticles as drug delivery system for stimuli-responsive controlled release, Carbon N. Y. 101 (2016) 135–142, https://doi.org/10.1016/j.carbon.2016.01.094.

[41] W.M. Qiao, Y. Song, S.Y. Lim, S.H. Hong, S.H. Yoon, I. Mochida, T. Imaoka, Carbon nanospheres produced in an arc-discharge process, Carbon N. Y. 44 (2006) 187–190, https://doi.org/10.1016/j.carbon.2005.07.016.

[42] P.V. Trinh, N.V. Chuc, B.H. Thang, P.N. Hong, P.N. Minh, Synthesis of uniform carbon mesospheres by arc discharge method 12 (2018) 484–488.

[43] D. Dorobantu, P.M. Bota, I. Boerasu, D. Bojin, M. Enachescu, Pulse laser ablation system for carbon nano-onions fabrication, Surf. Eng. Appl. Electrochem. 50 (2014) 390–394, https://doi.org/10.3103/S1068375514050044.

[44] S. Yang, H. Zeng, H. Zhao, H. Zhang, W. Cai, Luminescent hollow carbon shells and fullerene-like carbon spheres produced by laser ablation with toluene, J. Mater. Chem. 21 (2011) 4432–4436, https://doi.org/10.1039/c0jm03475d.

[45] J.A. Carrasco, H. Prima-Garcia, J. Romero, J. Hernández-Saz, S.I. Molina, G. Abellán, E. Coronado, CVD synthesis of carbon spheres using NiFe-LDHs as catalytic precursors: structural, electrochemical and magnetoresistive properties, J. Mater. Chem. C 4 (2016) 440–448, https://doi.org/10.1039/c5tc02861b.

[46] H.S. Qian, F.M. Han, B. Zhang, Y.C. Guo, J. Yue, B.X. Peng, Non-catalytic CVD preparation of carbon spheres with a specific size, Carbon N. Y. 42 (2004) 761–766, https://doi.org/10.1016/j.carbon.2004.01.004.

[47] X. Li, M. Chi, S.M. Mahurin, R. Liu, Y. Chuang, S. Dai, Z. Pan, Graphitized hollow carbon spheres and yolk-structured carbon spheres fabricated by metal-catalyst-free chemical vapor deposition, Carbon N. Y. 101 (2016) 57–61, https://doi.org/10.1016/j.carbon.2016.01.043.

[48] J.M. Keartland, D. Wamwangi, Generation of radical species in CVD grown pristine and N-doped solid carbon spheres using H2 and Ar as carrier gases 7 (2017) 21187–21195, https://doi.org/10.1039/c7ra03142d.

[49] Z. Wang, H. Ogata, G.J.H. Melvin, M. Obata, S. Morimoto, J. Ortiz-Medina, R. Cruz-Silva, M. Fujishige, K. Takeuchi, H. Muramatsu, T.Y. Kim, Y.A. Kim, T. Hayashi, M. Terrones, Y. Hashimoto, M. Endo, Structural evolution of hydrothermal carbon spheres induced by high temperatures and their electrical properties under compression, Carbon N. Y. 121 (2017) 426–433, https://doi.org/10.1016/j.carbon.2017.06.003.

[50] M. Zhang, H. Yang, Y. Liu, X. Sun, D. Zhang, D. Xue, Hydrophobic precipitation of carbonaceous spheres from fructose by a hydrothermal process, Carbon N. Y. 50 (2012) 2155–2161, https://doi.org/10.1016/j.carbon.2012.01.024.

[51] H. Wang, Q. Dai, Q. Li, J. Yang, X. Zhong, Y. Huang, A. Zhang, Z. Yan, Preparation of porous carbon spheres from porous starch, Solid State Ionics 180 (2009) 1429–1432, https://doi.org/10.1016/j.ssi.2009.08.006.

[52] L. Mao, Y. Zhang, Y. Hu, K.H. Ho, Q. Ke, H. Liu, Z. Hu, D. Zhao, J. Wang, Activation of sucrose-derived carbon spheres for high-performance supercapacitor electrodes, RSC Adv. 5 (2015) 9307–9313, https://doi.org/10.1039/C4RA11028E.

[53] S. Liu, X. Wang, H. Zhao, W. Cai, Micro/nano-scaled carbon spheres based on hydrothermal carbonization of agarose, Colloids Surfaces A Physicochem. Eng. Asp 484 (2015) 386–393, https://doi.org/10.1016/j.colsurfa.2015.08.019.
[54] C. Moreno-Castilla, Colloidal and micro-carbon spheres derived from low-temperature polymerization reactions, Adv. Colloid Interface Sci. 236 (2016) 113–141, https://doi.org/10.1016/j.cis.2016.08.003.
[55] Z.Q. Hao, J.P. Cao, Y. Wu, X.Y. Zhao, Q.Q. Zhuang, X.Y. Wang, X.Y. Wei, Preparation of porous carbon sphere from waste sugar solution for electric double-layer capacitor, J. Power Sources 361 (2017) 249–258, https://doi.org/10.1016/j.jpowsour.2017.06.086.
[56] J. Liu, S.Z. Qiao, H. Liu, J. Chen, A. Orpe, D. Zhao, G.Q. Lu, Extension of the Stöber method to the preparation of monodisperse resorcinol-formaldehyde resin polymer and carbon spheres, Angew. Chemie - Int 50 (2011) 5947–5951, https://doi.org/10.1002/anie.201102011.
[57] W. Stöber, A. Fink, E. Bohn, Controlled growth of monodisperse silica spheresin the micron size range, Jounal Colloid Interface Sci. 26 (1968) 62–69, https://doi.org/10.1016/0021-9797(68)90272-5.
[58] V.K. Saxena, U. Chandr, Microwave synthesis: a physical concept, microw. Heat, 1-21, https://doi.org/10.5772/22888, 2011.
[59] A. Díaz-Ortiz, P. Prieto, A. de la Hoz, A critical overview on the effect of microwave irradiation in organic synthesis,, Chem. Rec. 19 (2019) 85–97, https://doi.org/10.1002/tcr.201800059.
[60] A.S. Grewal, K. Kumar, S. Redhu, S. Bhardwaj, Microwave assisted synthesis: a green chemistry approach, Int. Res. J. Pharmaceut. Appl. Sci. 5 (2013) 278–285.
[61] Z. Lendzion-Bieluń, A. Wojciechowska, J. Grzechulska-Damszel, U. Narkiewicz, Z. Śniadecki, B. Idzikowski, Effective processes of phenol degradation on Fe3O4–TiO2 nanostructured magnetic photocatalyst, J. Phys. Chem. Solid. 136 (2020) 22–27, https://doi.org/10.1016/j.jpcs.2019.109178.
[62] M. Gaba, N. Dhingra, Microwave chemistry: general features and applications, Indian J. Pharm. Educ. Res. 45 (2011) 175–183.
[63] P. Staciwa, U. Narkiewicz, D. Sibera, D. Moszyński, R.J. Wróbel, R.D. Cormia, Carbon spheres as CO2 sorbents, Appl. Sci. 9 (2019) 3349–3369, https://doi.org/10.3390/app9163349.
[64] A. Majcher, J. Wiejak, J. Przybylski, T. Chudoba, J. Wojnarowicz, A novel reactor for microwave hydrothermal scale-up nanopowder synthesis, Int, J. Chem. React. Eng 11 (2013) 361–368, https://doi.org/10.1515/ijcre-2012-0009.
[65] S. Dąbrowska, T. Chudoba, J. Wojnarowicz, W. Łojkowski, Current trends in the development of microwave reactors for the synthesis of nanomaterials in laboratories and industries: a review,, Crystals 8 (2018), https://doi.org/10.3390/cryst8100379.
[66] A.W. Morawski, P. Staciwa, D. Sibera, D. Moszyński, M. Zgrzebnicki, U. Narkiewicz, Nanocomposite Titania−Carbon spheres as CO2 and CH4 sorbents, ACS Omega 5(4) (2020) 1966–1973, https://doi.org/10.1021/acsomega.9b03806.
[67] D. Sibera, J. Sreńscek-Nazzal, W.A. Morawski, B. Michalkiewicz, J. Serafin, R. J. Wróbel, U. Narkiewicz, Microporous carbon spheres modified with EDA used as carbon dioxide sorbents, Adv. Mater. Lett, 2018, pp. 432–435, https://doi.org/10.5185/amlett.2018.1872, 9(6).
[68] S. Kuśnieruk, J. Wojnarowicz, A. Chodara, T. Chudoba, S. Gierlotka, W. Lojkowski, Influence of hydrothermal synthesis parameters on the properties of hydroxyapatite nanoparticles, Beilstein J. Nanotechnol. 7 (2016) 1586–1601, https://doi.org/10.3762/bjnano.7.153.
[69] J. Wojnarowicz, T. Chudoba, S. Gierlotka, W. Lojkowski, Effect of microwave radiation power on the size of aggregates of ZnO NPs prepared using microwave solvothermal synthesis, Nanomaterials 8 (2018) 343–360, https://doi.org/10.3390/nano8050343.
[70] J. Wojnarowicz, M. Omelchenko, J. Szczytko, T. Chudoba, S. Gierlotka, A. Majhofer, A. Twardowski, W. Lojkowski, Structural and magnetic properties of Co-Mn codoped ZnO nanoparticles obtained by microwave solvothermal synthesis, Crystals 8 (2018) 410–438, https://doi.org/10.3390/cryst8110410.
[71] X. Liu, P. Song, J. Hou, B. Wang, F. Xu, X. Zhang, Revealing the dynamic formation process and mechanism of hollow carbon spheres: from bowl to sphere, ACS Sustain. Chem. Eng. 6 (2018) 2797–2805, https://doi.org/10.1021/acssuschemeng.7b04634.
[72] W. Kukułka, K. Wenelska, M. Baca, X. Chen, E. Mijowska, From hollow to solid carbon spheres: time-dependent facile synthesis, Nanomaterials 8 (2018) 861–872, https://doi.org/10.3390/nano8100861.
[73] G. Krishnamurthy, R. Namitha, Synthesis of structurally novel carbon micro/nanospheres by low temperature-hydrothermal process, J. Chil. Chem. Soc. 58 (2013) 1930–1933, https://doi.org/10.4067/S0717-97072013000300030.
[74] N.P. Wickramaratne, J. Xu, M. Wang, L. Zhu, L. Dai, M. Jaroniec, Nitrogen enriched porous carbon spheres: attractive materials for supercapacitor electrodes and CO2 adsorption, Chem. Mater. 26 (9) (2014) 2820–2828, https://doi.org/10.1021/cm5001895.
[75] N.P. Wickramaratne, V.S. Perera, J.M. Ralph, S.D. Huang, M. Jaroniec, Cysteine-assisted tailoring of adsorption properties and particle size of polymer and carbon spheres, Langmuir 29 (12) (2013) 4032–4038, https://doi.org/10.1021/la400408b.
[76] J. Ludwinowicz, M. Jaroniec, Potassium salt-assisted synthesis of highly microporous carbon spheres for CO2 adsorption, Carbon 82 (2015) 297–303, https://doi.org/10.1016/j.carbon.2014.10.074.
[77] C. Scherdel, T. Scherb, G. Reichenauer, Spherical porous carbon particles derived from suspensions and sediments of resorcinol–formaldehyde particles, Carbon 47 (9) (2009) 2244–2252, https://doi.org/10.1016/j.carbon.2009.04.015.
[78] N. Rey-Raap, S.F. Villanueva, J. Angel Menéndez, A. Arenillas, Microporous carbon spheres derived from resorcinol-formaldehyde solutions. A new approach to coat supports, Micropor. Mesopor. Mater 252 (2017) 154–160, https://doi.org/10.1016/j.micromeso.2017.06.018.
[79] S. Xu, C. Liu, F. Ye, Y. Guo, J. Wiezorek, Alkali-assisted hydrothermal route to control submicron-sized nanoporous carbon spheres with uniform distribution, Colloids Surfaces A Physicochem. Eng. Asp 515 (2017) 1–11, https://doi.org/10.1016/j.colsurfa.2016.11.070.
[80] V. Datsyuk, M. Kalyva, K. Papagelis, J. Parthenios, D. Tasis, A. Siokou, I. Kallitsis, C. Galiotis, Chemical oxidation of multiwalled carbon nanotubes, Carbon N. Y. 46 (2008) 833–840, https://doi.org/10.1016/j.carbon.2008.02.012.
[81] J.W. Long, M. Laskoski, T.M. Keller, K.A. Pettigrew, T.N. Zimmerman, S.B. Qadri, G.W. Peterson, Selective-combustion purification of bulk carbonaceous solids to produce graphitic nanostructures, Carbon N. Y. 48 (2) (2010) 501–508, https://doi.org/10.1016/j.carbon.2009.09.068.
[82] M. Thommes, K. Kaneko, A.V. Neimark, J.P. Olivier, F. Rodriguez-Reinoso, J. Rouquerol, K.S.W. Sing, Physisorption of gases, with special reference to the evaluation of surface area and pore size distribution (IUPAC Technical Report), Pure Appl. Chem. 87 (2015) 1051–1069, https://doi.org/10.1515/pac-2014-1117.
[83] S. Lowell, J.E. Shields, M. A. Thomas, M. Thommes, Characterization of porous solids and powders: surface area, pore size and density, particle technology series, SPRINGER SCIENCE+BUSINESS MEDIA, LLC.
[84] Z. Lendzion-Bielun, L. Czekajlo, D. Sibera, D. Moszynski, J. Srenscek-Nazzal, R. Wrobel, B. Michalkiewicz, W. Arabczyk, U. Narkiewicz, Surface characteristics of KOH-treated commercial carbons applied for CO2 adsorption, Adsorpt. Sci. Technol. 36 (1–2) (2018) 478–492, https://doi.org/10.1177/0263617417704527.
[85] D. Lozano-Castelló, D. Cazorla-Amorós, A. Linares-Solano, Usefulness of CO_2 adsorption at 273 K for the characterization of porous carbons, Carbon N. Y. 42 (7) (2004) 1233–1242, https://doi.org/10.1016/j.carbon.2004.01.037.
[86] J. Silvestre-Albero, A. Wahby, A. Sepúlveda-Escribano, M. Martínez-Escandell, K. Kaneko, F. Rodríguez-Reinoso, Ultrahigh CO_2 adsorption capacity on carbon molecular sieves at room temperature, Chem. Commun. 47 (2011) 6840–6842, https://doi.org/10.1039/c1cc11618e.
[87] V. Presser, J. McDonough, S.H. Yeon, Y. Gogotsi, Effect of pore size on carbon dioxide sorption by carbide derived carbon, Energy Environ. Sci. 4 (2011) 3059–3066, https://doi.org/10.1039/c1ee01176f.
[88] G. Sethia, A. Sayari, Comprehensive study of ultra-microporous nitrogen-doped activated carbon for CO_2 capture, Carbon N. Y. 93 (2015) 68–80, https://doi.org/10.1016/j.carbon.2015.05.017.
[89] M. Sevilla, A.B. Fuertes, Sustainable porous carbons with a superior performance for CO2 capture, Energy Environ. Sci. 4 (2011) 1765–1771, https://doi.org/10.1039/C0EE00784F.
[90] S.Y. Lee, S.J. Park, Determination of the optimal pore size for improved CO_2 adsorption in activated carbon fibers, J. Colloid Interface Sci. 389 (2013) 230–235, https://doi.org/10.1016/j.jcis.2012.09.018.
[91] L.K.C. De Souza, N.P. Wickramaratne, A.S. Ello, M.J.F. Costa, C.E.F. Da Costa, M. Jaroniec, Enhancement of CO_2 adsorption on phenolic resin-based mesoporous carbons by KOH activation, Carbon N. Y. 65 (2013) 334–340, https://doi.org/10.1016/j.carbon.2013.08.034.
[92] N.P. Wickramaratne, M. Jaroniec, Importance of small micropores in CO_2 capture by phenolic resin-based activated carbon spheres, J. Mater. Chem. A 1 (2013) 112–116, https://doi.org/10.1039/c2ta00388k.
[93] L. Chen, T. Watanabe, H. Kanoh, K. Hata, T. Ohba, Cooperative CO_2 adsorption promotes high CO_2 adsorption density over wide optimal nanopore range, Adsorpt. Sci. Technol. 36 (2018) 625–639, https://doi.org/10.1177/0263617417713573.
[94] D.M. D'Alessandro, B. Smit, J.R. Long, Carbon dioxide capture: prospects for new materials, Angew. Chemie - Int 49 (2010) 6058–6082, https://doi.org/10.1002/anie.201000431.
[95] T.J. Bandosz, M. Seredych, E. Rodríguez-Castellón, Y. Cheng, L.L. Daemen, A. J. Ramírez-Cuesta, Evidence for CO_2 reactive adsorption on nanoporous S- and N-doped carbon at ambient conditions, Carbon N. Y. 96 (2016) 856–863, https://doi.org/10.1016/j.carbon.2015.10.007.